Journal of Colloid and Interface Science 629 (2023) 265–275

Contents lists available at ScienceDirect

Journal of Colloid and Interface Science

journal homepage: www.elsevier.com/locate/jcis

Impact of organic solutes on capillary phenomena in water-CO_2-quartz systems

Emily Wei-Hsin Sun *, Ian C. Bourg

Department of Civil and Environmental Engineering and High Meadows Environmental Institute, Princeton University, Princeton, NJ 08544, United States

GRAPHICAL ABSTRACT

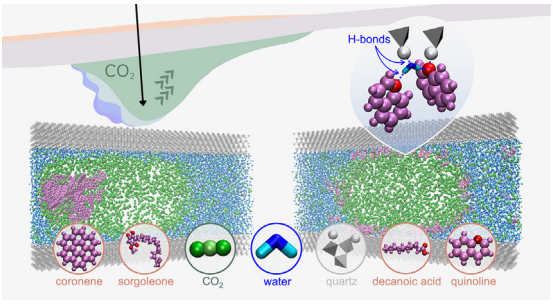

ARTICLE INFO

Article history:
Received 16 June 2022
Revised 17 August 2022
Accepted 18 August 2022
Available online 23 August 2022

Keywords:
Wettability
Capillarity
Multi-phase flow
Interfacial tension
Disjoining pressure
Contact angle
Curvature
Carbon capture and storage
Molecular dynamics

ABSTRACT

Hypothesis: The migration of supercritical CO_2 ($scCO_2$) injected into underground reservoirs as part of carbon capture and storage is influenced by organic contamination affecting mineral wettability. Molecular dynamics (MD) simulations of relevant systems that incorporate representative organic solutes allow detailed investigation of changes in fundamental interfacial and capillary properties. *Experiments*: We use MD simulations to explore the effects of four organic solutes (quinoline, decanoic acid, coronene, sorgoleone) on the wettability of quartz by water in the presence of $scCO_2$. We examine the impacts of polar, alkyl, and aromatic moieties as well as fluid flow velocity at elevated temperatures and pressures. *Findings*: Organic molecules accumulate at the water-CO_2 interface, where they distribute according to their size and functional groups. Certain organics penetrate the adsorbed water film at the quartz-CO_2 interface, revealing two modes of hydrogen bonding between polar organic functional group, water, and quartz surface –OH groups. Interfacial energies and contact angles are minimally impacted by organic adsorption at the water-CO_2 interface, possibly due to simultaneous CO_2 desorption. Non-equilibrium MD simulations reveal that flow-induced redistribution of organic compounds modulates the radii of curvature of the advancing and receding water-CO_2 interfaces. Our results indicate that organic adsorption on water surfaces is likely ubiquitous during multi-phase flow in soils and sedimentary rocks, with implications for the mobilization and transport of organic compounds.

Abbreviations: BECCS, bioenergy with carbon capture and storage; CDR, carbon dioxide removal; DACCS, direct air capture and carbon capture and storage; EOR, enhanced oil recovery; GCS, geologic carbon storage; GHG, greenhouse gas; MD, molecular dynamics; NEMD, non-equilibrium molecular dynamics; scCO2, supercritical carbon dioxide; Γ, surface excess; γ, interfacial tension; θ, contact angle; Φ, ratio of organic matter at the receding and advancing ends of the CO2 bubble.

* Corresponding author at: 59 Olden Street, Princeton University Engineering Quad. E-209, Princeton, NJ 08544, USA.
E-mail addresses: esun@princeton.edu (E.W.-H. Sun), bourg@princeton.edu (I.C. Bourg).

https://doi.org/10.1016/j.jcis.2022.08.124
0021-9797/

1. Introduction

As human activities increasingly perturb Earth's climate, carbon dioxide removal (CDR) technologies have emerged as playing a necessary role in achieving the deep reductions of greenhouse gas (GHG) emissions necessary to mitigate adverse impacts and irreversible changes across the globe [1–3]. In almost all climate scenarios modeled and assessed by the IPCC, including every pathway that limits global warming to 1.5–2 °C, CDR approaches are necessary to reach global net zero or net-negative GHG emissions. Several CDR approaches, including bioenergy with carbon capture and storage (BECCS) and direct air capture and carbon capture and storage (DACCS), involve geologic carbon storage (GCS), whereby supercritical CO_2 ($scCO_2$) is trapped in geologic formations. These methods are potentially permanent barring leakage and have large sequestration potentials of several $GtCO_2$ per year [4].

Secure trapping relies on the ability to predict the flow of $scCO_2$ through the porous sedimentary rocks that typically make up storage reservoirs [5]. In two of the most important trapping mechanisms, stratigraphic (or structural) trapping and residual (or capillary) trapping, the flow and distribution of $scCO_2$ depends on the wettability of the mineral surfaces by water versus $scCO_2$ [6–9]. In stratigraphic trapping, the migration of $scCO_2$ plumes through fine-grained seals or caprocks is blocked by high capillary entry pressure [10–12]. In residual trapping, plumes of $scCO_2$ are fragmented into immobile disconnected ganglia [13,14]. For both trapping mechanisms, water wettability of the mineral surfaces impacts storage capacity and can be characterized by the contact angle (θ) of water and $scCO_2$ with mineral surfaces [15–18]. While θ values are a fundamental determining parameter for predicting the distribution of $scCO_2$ plumes in GCS, θ observations remain varied, ranging from 0° (strongly water-wet) to around 110° (mildly CO_2-wet) [19–22]. These variations are important to understand as general thresholds indicate that stratigraphic trapping is compromised at θ values greater than 90°, and residual trapping and drainage are affected when θ values are around or above 50° [23,24].

One oft-cited potential cause of measurement variability is contamination by impurities altering surface roughness or modifying interfacial energies [20,25]. In deep saline aquifers and caprocks, organic compounds that adhere to mineral surfaces through electrostatic, hydrophobic, or covalent interactions have been shown to increase observed θ values, making systems more hydrophobic and reducing residual CO_2 trapping capacity [26–40]. Despite agreement on the potential for organics to affect wetting and numerous empirical and theoretical studies, there remain knowledge gaps regarding the driving mechanisms—such as steric effects, enthalpic or entropic contributions to water film disruption, organic polarity effects, surface roughness changes, or CO_2 adhesion—dominating organic equilibration between phases and surface hydrophilicity changes [19,41–46]. A more detailed understanding of the influence of organic compounds on wettability in GCS conditions can help improve our understanding of rock-fluid interactions and our predictions of reservoir capacities.

Molecular dynamics (MD) simulation methods are well-suited to complement established micro- and nano-scale experimental techniques by examining the emergence of wetting and capillary properties (contact angles, adsorbed fluid films) from atomistic-level interactions in systems that contain solid surfaces and multiple fluids [47–53]. Simulation studies on the impact of organics on mineral wettability in environments relevant to GCS typically alter the mineral surfaces directly, either by grafting organic chains to the surface or by modulating the parameters characterizing the surface [54,55]. These studies have provided detailed evidence that silica surfaces functionalized to mimic organic chemisorption (through replacement of silanol groups with hydrophobic organic functional groups) exhibit a less hydrophilic character. Other MD simulation studies involving organics near mineral surfaces in the presence of either water or CO_2 have provided significant information on organic aggregation, distribution, and diffusion in water or brine [56–64]. To our knowledge, however, there are currently no high temperature and pressure MD simulation studies on capillary phenomena that model free organics in systems containing bulk-fluid-like water and CO_2 near mineral surfaces.

In a recent study, we carried out a detailed examination of capillary phenomena associated with the coexistence of $scCO_2$ and water in a silica nanopore [65]. In particular, we characterized the relationship between the distribution of the fluid phases (interface curvature, contact angle, adsorbed film thickness) and the capillary pressure difference between water and $scCO_2$. Here, we build on our previously developed methodologies to explore how the inclusion of organic compounds affects capillary and multiphase flow properties. We examine four different organic molecules with varying levels of polarity, size, and shape representing diverse and relevant functional groups including alkyl chains, polyaromatic and heterocyclic rings, quinones, carboxylic acids, and amines (Fig. 1). We allow relatively long equilibration times relative to previous MD simulations of mineral wettability by water vs $scCO_2$ and generate the first model observations of free organics (vs organics grafted to the mineral surface) in the presence of water and $scCO_2$ in a quartz nanopore. Although our simulations are designed to probe conditions relevant to GCS, we note that questions related to the influence of organic compounds on wettability and capillary phenomena recur frequently in soil science, [66] atmospheric chemistry, [67] materials science, [68] biology, [69] water purification technology, [70] and other fields [71].

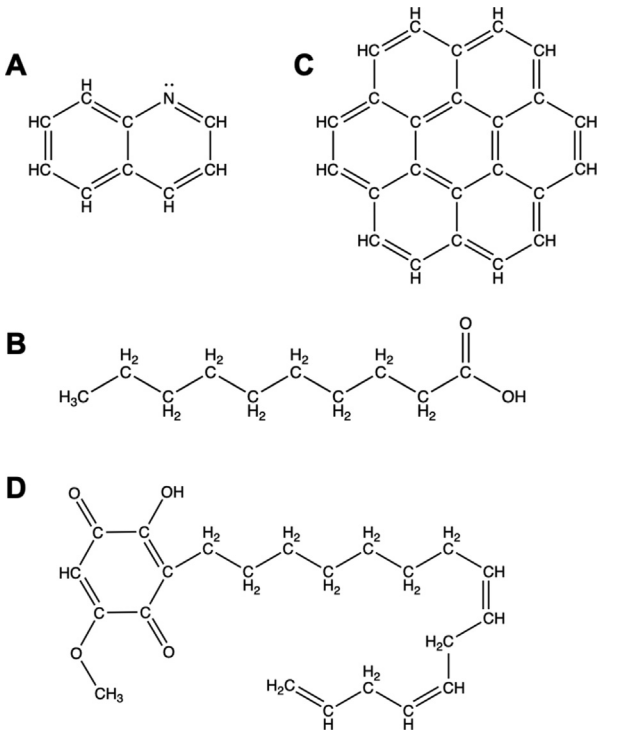

Fig. 1. Chemical structures of the organic molecules considered in this study: (A) quinoline, (B) decanoic acid, (C) coronene, and (D) sorgoleone.

2. Materials and methods

2.1. Model structure

Sandstone formations and fine-grained sedimentary caprocks both typically contain a substantial amount of quartz, [33,72–76] and the wetting properties of quartz and sandstone have been shown to be comparable [9,77]. The quartz unit cell used in this study was based on X-ray diffraction analyses by Kihara, [78] with the surface prepared by cleaving bulk quartz along the stable "termination β" (10$\bar{1}$0) plane as described in Sun et al. [65,79]. The protonation and hydroxylation of undercoordinated oxygen and silicon atoms results in a surface silanol site density of 7.53 OH per nm^2 and a neutral surface charge.

The full slab of α-quartz has dimensions of 176.89 × 4.04 × 27.02 Å (36 × 8 × 5 unit cells) forming parallel surfaces in the $x-z$ plane spaced 66 Å apart across a slit-shaped nanopore filled with water and CO_2. The full simulation cell size is 176.89 × 100.00 × 27.02 Å with periodic boundary conditions in every direction. The shorter depth along the z axis creates a system with two-dimensional fluid–fluid curvature in the $x-y$ plane, thus avoiding three-phase line tension and its effects on the contact angle [80–82].

The organic molecules considered in this study were quinoline (C_9H_7N), decanoic acid ($C_{10}H_{20}O_2$), coronene ($C_{24}H_{12}$), and sorgoleone ($C_{22}H_{30}O_4$) (Fig. 1). These compounds represent typical organic functional groups present in crude oil and aquifers and were chosen to highlight the roles of polarity, aromaticity, and size in altering capillary properties [83]. Quinoline exhibits relatively high solubility in water and thus has particular environmental significance [84]. It has been identified in shale oil extraction waste materials and represents the polar and aromatic components of crude oil [85,86]. Decanoic acid has been used in previous studies to represent the carboxylic acid components of crude oil and can also be present in novel solvents for the capture stage of CCS [64,87]. Coronene is a proxy for polyaromatics that are abundant in the subsurface [88] and has been used in previous studies to represent hydrocarbons in shale [89]. Sorgoleone was selected as a larger amphiphilic organic molecule with both quinone and alkyl functional groups. The low pH condition implied by the hydroxylation of undercoordinated oxygen and silicon atoms on the quartz surface determines the protonation state of the organic molecules (Table 1). Each protonation state was chosen in the approximate pH range of 3 to 6 to avoid necessitating the addition of counterions in this study. This range is expected in the presence of $scCO_2$ over time, with pH lowering quickly upon introduction of $scCO_2$ and then incompletely buffering in the presence of carbonates and aluminosilicates [26,74–76,90]. The initial structure for each organic molecule was created using Avogadro 1.2.0.

The highest pressure model structures in our previous study were edited using a script that deletes water and CO_2 molecules that overlap with inserted organic molecules. With water-CO_2 interfaces initially flat and oriented normal to the quartz surface, organic molecules were inserted along the quartz surfaces as a monolayer and the number of water and CO_2 molecules corresponding to the space taken up by the organic molecules was removed (Figure S1 showing initial configuration). This resulted in a variety of molecule numbers and pressures based on the size and width (in the y direction) of the organic molecules (Table S1). The insertion of the organics along the quartz surfaces was carried out to mimic an initially organic-coated mineral surface. However, as shown below, in all simulations organic molecules rapidly rearranged to the fluid–fluid interface. If the organic compounds were uniformly dissolved in the aqueous phase in our simulations, the ratio of organic to water molecules would yield average concentrations of 1.24, 1.21, 0.68, and 0.79 M for quinoline, decanoic acid, coronene, and sorgoleone, respectively, much higher than the concentrations of dissolved organic matter observed in deep saline aquifers (~0.01 M) or depleted oil reservoirs, except where 'slugs' of organic matter are mobilized [26,41]. However, the organic compounds accumulate strongly at the fluid–fluid interfaces in our simulations, such that their concentration in the bulk aqueous phase is low, on the order of 0.001 to 0.05 M.

Table 1
Properties of the four simulated organics.

	Mass (Da)	pKa	Aqueous solubility (mg/dm^3)
Quinoline	129.2	4.90[91]	6110[91]
Decanoic acid	172.3	4.90[92]	61.8[92]
Coronene	300.4	–	0.00014[93]
Sorgoleone	358.5	6.0[94]	0.04[95]

2.2. Interatomic potential parameters

As in our previous study, we employed the CLAYFF force field for quartz, [96] the extended simple point charge (SPC/E) model for water, [97] the elementary physical model 2 (EPM2) model for CO_2, [98] and the optimized potentials for liquid simulations all-atom (OPLS-AA) model for organics [99]. The specific parameters for atoms, bonds, angles, and dihedrals in the organic molecules were assigned using the Moltemplate molecule builder [100]. Lorentz-Berthelot combining rules were used to calculate interactions between unlike atoms, except interactions between CO_2 and water or quartz O atoms, for which the PPL model was used [101]. We note that the quality of MD simulation predictions is inherently sensitive to the choice of interatomic potential models. To the best of our knowledge, a well-tested combination of interatomic potential models does not exist for systems that contain all four components examined in this study (i.e., water, CO_2, organic matter, and quartz). However, the force fields used here have been extensively validated against experimental properties of systems that contain one, two, or three of these four components, including pure water, [102–104] pure CO_2, [65,105] quartz/silica-water, [106,107] water-CO_2, [80,108,109] water-organic, [110] quartz-water-CO_2, [65,111] and mineral–water-organic systems [112]. In particular, our previous study demonstrated accurate predictions of the CO_2 equation of state, water-CO_2 interfacial energy, and CO_2 adsorption at the water-CO_2 interface, and yielded results consistent with the experimental database on water-CO_2 contact angles on stringently cleaned quartz surfaces [65]. With the inclusion of organics, the CO_2 equation of state remains reproducible (Figure S2).

The silicon and oxygen atoms of the quartz slab were constrained to avoid distortion. Water molecules were kept rigid using the SHAKE algorithm, and CO_2 and organic molecules were modeled as flexible. Short-range Coulomb and van der Waals interactions were truncated at 12 Å. Long-range Coulomb interactions were treated by three-dimensional PPPM summation. In our previous paper, this combination of models accurately described the structure and dynamics of water and CO_2 at various pressures, although it overestimated the solubility of CO_2 in water [65]. All interatomic interaction parameters are summarized in Table S2.

2.3. Equilibrium simulation details

All MD simulations used the open-source program LAMMPS [113]. Simulations were initialized with an energy minimization run in the microcanonical (*NVE*) ensemble to reduce excessive and artificial forces. These brief runs were followed by equilibration runs in the canonical (*NVT*) ensemble at 318 K for 25 to

70 ns. The simulations were determined to be at equilibrium when bulk fluid properties became isotropic, adsorbed water films at the quartz-CO_2 interface attained a stable thickness, potential energy converged, and organic molecules reached a steady distribution. The larger organic molecules, coronene and sorgoleone, migrated along the water-CO_2 interface to aggregate into a distinct organic phase, taking longer to reach an equilibrium configuration. Finally, each system was simulated for additional 20 ns production runs in the canonical (*NVT*) ensemble to sample equilibrium properties. The overall duration of our equilibration and production runs was similar or longer than that used in all previous studies of wettability in mineral–water-CO_2 systems to the best of our knowledge [54,80,114]. All simulations were run at 318 K. The temperature was kept constant using a Nosé-Hoover thermostat with a coupling constant of 1 ps.

2.4. Non-equilibrium simulation details

Following the equilibrium production runs, a force in the x direction was added to every atom of the fluid components in each system to induce multiphase flow within the quartz nanopore. The amount of force added can be translated to a force density, which is analogous to a pressure gradient. For each system, simulations were carried out with CO_2 bubble velocities of 1, 2, or 4 nm ns^{-1} using force densities on the order of 10^5 Pa nm^{-1} as reported in Table S3. As commonly implemented in such non-equilibrium MD (NEMD) simulations, the force densities applied in our systems are extremely high (relative to natural systems) due to the large fluid velocities required to visualize flow over nanosecond time scales. To facilitate the computations of average atomic density maps, an opposite and equivalent motion for every atom of the solid component in each system was added at constant velocities of 1, 2, or 4 nm ns^{-1}. These positional updates create an opposing force that prevents the CO_2 bubble from moving through the periodic boundary (video provided in the Supplementary Materials).

2.5. Analysis

Densities and stresses were collected as a function of the $x-y$ coordinates with a 1×1 Å resolution using LAMMPS. All further analyses and calculations were performed using Python 3.8.5, Jupyter Notebook 6.1.4, and Visual Molecular Dynamics (VMD) 1.9.4. Data points were collected from time-averaged maps of the densities and stresses every 5 ns within the 20 ns production runs from data recorded every 1 fs.

Interface locations were calculated using Gibbs' definition of the location yielding a zero surface excess of water. At least 10 Å away from any of these interfaces, bulk regions were defined as 20×40 Å regions in the xy plane displaying isotropic stress tensors. Bulk pressures, densities, and water density profiles matched well with previously validated simulations. Water density layering with ~ 3 Å spacing is observed within ~ 10 Å from the quartz surface, and these profiles were used to determine the existence and width of the adsorbed water layer stabilized by the evenly distributed surface silanol groups. All structural and energetic properties were compared to the systems without any organics explored in our previous study [65].

2.6. Visualization

Molecular trajectories were visualized using VMD 1.9.4 using gray polyhedra to represent quartz tetrahedra, white to represent silanol hydrogens, light and dark blue to represent water H and O atoms, light and dark green to represent CO_2 C and O atoms, pink to represent organic C and H atoms, and red to represent organic O and N atoms (Fig. 2). The general color scheme of green for CO_2, blue for water, and red for organic molecules remains consistent for all figures showing atomic densities and stresses of each component.

3. Results and discussion

3.1. Equilibrium structural properties

For all systems, the density distribution of bulk water near the quartz surface remained the same as in previous studies without organics, showing three hydration layers, one located at 3 ± 0.5 Å above the average height of the silanol O atoms followed by layers at 6 ± 0.5 Å and 10 ± 0.5 Å. The quartz-water interface location, 1.4 Å above the silanol O atoms, is in agreement with the 1.5 Å radius of O atoms. For all systems, the adsorbed water film between the quartz and CO_2 phase is composed of ~ 1.5 water monolayers and the first water layer has a structure analogous to that of bulk water near quartz. These films are analyzed in further detail in a subsequent section.

Organic molecules examined in this study distribute in two main ways, either coating the water-CO_2 interface or collecting into their own phase. Quinoline distributes evenly along the water-CO_2 interface. Its polarity lends it a relatively higher solubility in water, which is displayed by the presence of small amounts dissolved in the bulk water phase and within the thin adsorbed film. Decanoic acid also distributes evenly along the water-CO_2 interface, with its polar head group oriented strongly towards the water and its hydrophobic alkyl chain protruding into the CO_2 phase. Coronene is the least polar of the organic molecules studied here and aggregates into its own spherical (or cylindrical) phase. It rests mainly in the CO_2 phase, accumulating in a concave region of the water surface. Likewise, sorgoleone forms its own phase. However, whereas coronene forms an aggregate that tends to minimize the surface area of the coronene phase, sorgoleone forms an aggregate that conforms to the shape of the water-CO_2 interface, suggesting a weaker tendency towards self-attraction vs attraction to the water surface. Despite the very low solubilities of coronene and sorgoleone, none of the organic compounds displayed an affinity for the quartz surface. These observations agree with studies showing that quartz is less likely than other minerals to adsorb organics, especially those that are neutral, and does not promote as thick a layer of adsorbed organics as other minerals like mica or carbonates [38,115]. The movement of organic molecules away from the mineral surface during equilibration also reflects behavior observed in organic aggregation and oil detachment studies related to CO_2-enhanced oil recovery (EOR) [61]. Either due to the existence of more polar groups or due to Van der Waals attraction to the denser water phase, all four molecules present strong tendencies to either adsorb or aggregate at the water-CO_2 interface and thus tend to disrupt the distribution of CO_2 near the water surface. These distributions, as well as the corresponding water and CO_2 density maps, are shown in Fig. 3.

Results from our previous study (obtained in the absence of organic compounds) showed that the thickness of the water film is sensitive to the disjoining pressure in the film – or, equivalently, to the capillary pressure difference between the bulk water and CO_2 phases [65]. Results obtained in the presence of organic compounds are plotted as a function of disjoining pressure in Fig. 4 (brown symbols) for comparison with film thicknesses obtained without organic molecules (gray symbols). While all film thicknesses fall within the quartile ranges of those in systems without organics at similar pressures, both the quinoline and decanoic acid systems have statistically significant departures from the thicknesses expected in systems without organics. The mean film thickness in the system with quinoline molecules is significantly

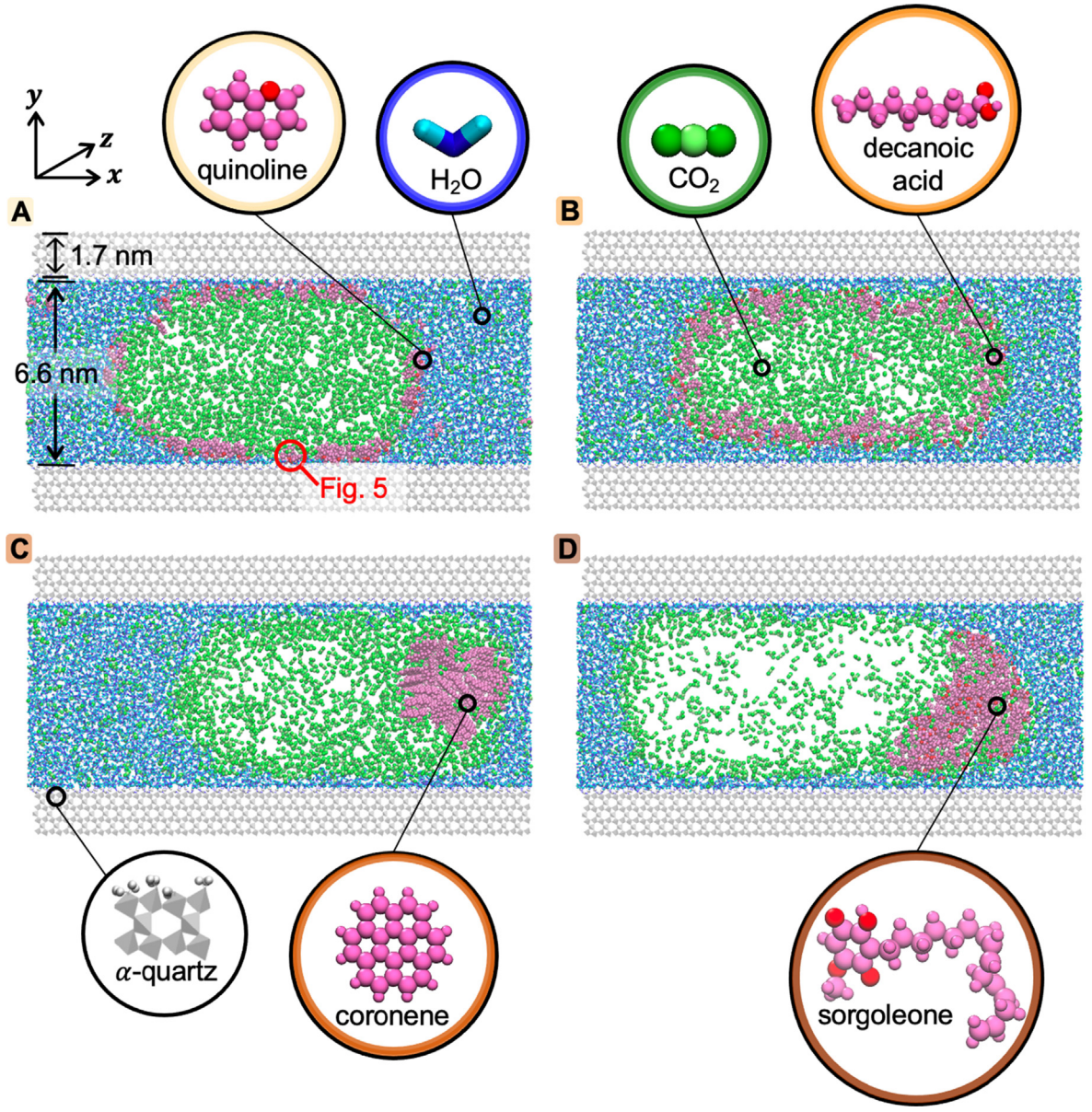

Fig. 2. Snapshots of each simulated system at equilibrium, with magnified snapshots of each component. Each equilibrated system involves a different organic molecule: (A) quinoline, (B) decanoic acid, (C) coronene, and (D) sorgoleone. The magnified snapshots show water, CO_2, quartz, and organics with small black circles marking their location in the full system. A small red circle in panel A marks the location of the quinoline-water–quartz hydrogen bond interactions highlighted in Fig. 5. (For interpretation of the references to color in this figure legend, the reader is referred to the web version of this article.)

smaller than in systems without organics at a similar disjoining pressure (that shown at 5.9 MPa in Fig. 4), with over 19 % difference outside of the expected range. This significance is likely larger when compared to data without organics extrapolated to lower disjoining pressures closer to that in the simulation with quinoline. On the other hand, the mean film thickness in the system with decanoic acid molecules is significantly larger than in systems without organics at a similar disjoining pressure, with a 34 % difference outside of the expected range. Coronene and sorgoleone had insignificant impacts on film thickness, as expected from their accumulation in curved regions of the water-CO_2 interface rather than on the flat surface of the adsorbed water film.

Our results reveal that decanoic acid at the quartz surface draws more water into the adsorbed film, as expected of surfactant-like molecules, [116] while quinoline destabilizes the film. This significant disruption of the water film by quinoline may be due to hydrogen bonds formed by quinoline with the quartz surface that are absent from interactions with decanoic acid (Fig. 5A). Simulation snapshots confirm two different modes of hydrogen bonds between quinoline and the quartz surface silanol groups resembling those of inner- and outer-sphere surface complexes. The density profile of the quinoline N atoms (Fig. 5B) clearly shows the appearance of two tight peaks, one 3.5 Å from the quartz silanol O atom (the inner-sphere 1° mode) and another 6.5 Å from the quartz silanol O atom (the outer-sphere 2° mode). The 3 Å spacing between the two modes of bonding corresponds to the width of one water layer. Notably, 1° and 2° modes of hydrogen bonding can exist concurrently on the same N atom, and the 2° mode may facilitate the 1° mode. The density profile peaks also show that the 1° mode of hydrogen bonding occurs within the adsorbed water layer (the shaded blue area between vertical dashed blue lines in Fig. 5B), thus disrupting the water film. In the 2° mode, quinoline N atoms remain outside of the adsorbed water film, in the CO_2 phase (the shaded green area in Fig. 5B), but their proxim-

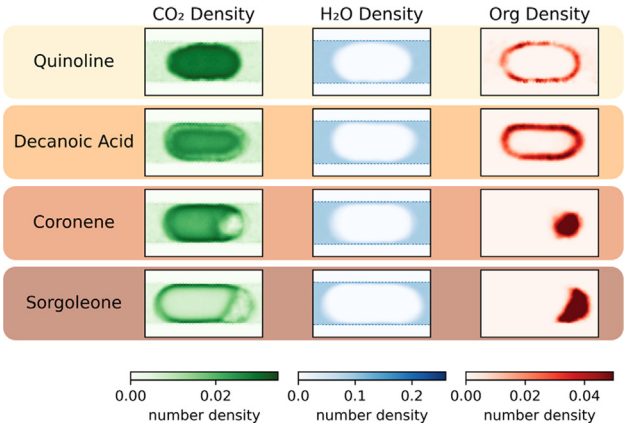

Fig. 3. Atomic density maps showing CO_2 (green), water (blue), and organic densities (red) in the $x-y$ plane for each system at equilibrium. (For interpretation of the references to color in this figure legend, the reader is referred to the web version of this article.)

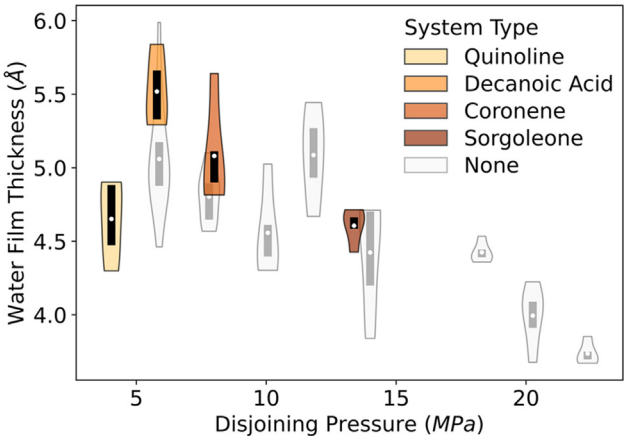

Fig. 4. Violin plot showing the thickness of the water film adsorbed at the quartz-CO_2 interface as a function of disjoining pressure. Results presented from lighter to darker brown colors were obtained in the presence of organics of increasing molecular weight. Results obtained without organics in our previous study are presented in gray.

ity and the orientation of the quinoline molecules may still lead to some steric disruption of the water film. Water molecules have a strong preference to form hydrogen bonds with each other and silanol groups at the interface [117]. Quinoline is the only molecule in our study that displays an analogous behavior. This suggests that certain compounds may be more likely to penetrate the structured water layers and promote surface de-wetting without necessarily undergoing chemisorption to the mineral surface. Moreover, attraction to the water-CO_2 interface brings these organics into increased contact with the thin water film where unique geochemistry could potentially enhance reactivity not studied here [118].

We quantify the surface excesses of CO_2 and organic solutes (Γ_g and Γ_{org}) at the curved water-CO_2 interface. Resulting Γ_g-values are presented in Fig. 6 in the absence and presence of organics. Results on Γ_{org} are presented in a more detailed figure in the supporting information (Figure S3). As shown by the gray symbols in Fig. 6, in the absence of organics, CO_2 showed significant adsorption at the water-CO_2 interface, with the greatest Γ_g-values observed at or near the critical pressure of CO_2. In the presence of organics, our results show that at the two surfaces with no organic accumulation (i.e., coronene and sorgoleone on the left curved interface), Γ_g is consistent with that observed in the

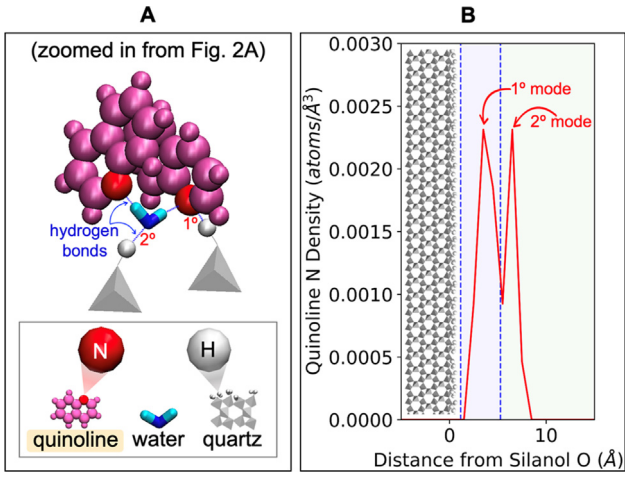

Fig. 5. Panel A: Detailed view of the region circled in red in Fig. 2A showing two quinoline molecules (pink and red) forming two types of hydrogen bonds (blue dashed lines) with the quartz surface (gray tetrahedra). The quinoline molecule on the left forms a hydrogen bond with a water molecule that is hydrogen bonded to a quartz silanol hydroxyl. The quinoline molecule on the right directly receives a hydrogen-bond from a quartz silanol group. Panel B: Average density profile of quinoline N atoms along a transect in the middle of the water film relative to the plane of quartz silanol O atoms. Vertical dashed blue lines show the positions of the quartz-water and water-CO_2 interfaces. (For interpretation of the references to color in this figure legend, the reader is referred to the web version of this article.)

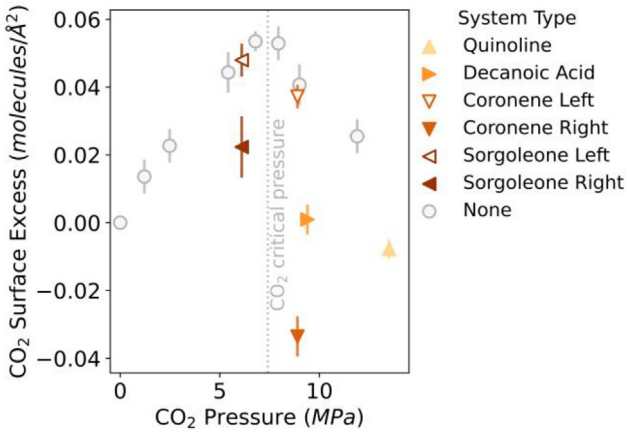

Fig. 6. Surface excess of CO_2 at the curved water-CO_2 interface (quantified at the pore mid-plane from the density profiles presented in Figure S4) as a function of CO_2 pressure. Results obtained in our previous study in the absence of organics are shown as gray circles. The CO_2 critical pressure is indicated as a dotted gray vertical line.

absence of organics. At all other curved water-CO_2 interfaces, we observe a significant decrease in Γ_g associated with organic adsorption (Fig. 6).

Overall, we find that the strong adsorption of all four organics at the water-CO_2 interface is accompanied by CO_2 desorption (i.e., by a decrease in Γ_g). A rough translation of our Γ_g and Γ_{org}-values into an 'equivalent thickness' of adsorbed organic matter and CO_2 (based on the volume of each molecule) reveals that in the case of quinoline or decanoic acid, where the organics uniformly coat the water surface, organic adsorption displaces a roughly equivalent volume of adsorbed CO_2. More precisely, for the quinoline system, the equivalent thickness of adsorbed CO_2 and organics (2.2 ± 0.4 Å) matches the value observed without organics at the nearest CO_2 pressure (1.9 ± 0.4 Å). Similarly, for the decanoic acid system, the equivalent thickness of adsorbed CO_2 and organics (3.

7 ± 0.6 Å) matches the value observed without organics at the nearest CO_2 pressure (3.0 ± 0.5 Å). These observations suggest that the displacement of adsorbed CO_2 by adsorbed organic molecules can be viewed, at least in certain cases where organics adsorb evenly at the water-CO_2 interface, as a simple volumetric replacement. For the systems with coronene and sorgoleone, where the organics aggregate into their own phase on one side of the water-CO_2 interface, calculated surface excesses are less meaningful as the organic compounds have a non-uniform thickness on the water surface, and more complex behaviors are observed including evidence of CO_2 accumulation at both the CO_2-organic and the organic-water interfaces. Additional complications are expected in systems where organics have affinity for the mineral surface. However, little evidence of such affinity was observed in our simulated systems (beyond the weak affinity of quinoline molecules for surface silanol groups noted above), perhaps because of the strongly hydrophilic nature of the quartz surface and the neutral character of the organic compounds [115].

3.2. Equilibrium thermodynamic properties

As in our previous study, we use the anisotropy of the local stress tensor at the pore mid-plane (dashed line in Figure S4) to determine the interfacial tension at the curved water-CO_2 interface, γ_{gw}.[65] Results are presented in Fig. 7A. While both quinoline and decanoic acid result in γ_{gw} values on the lower end of the range expected based on systems without organics, neither difference is statistically significant. This finding differs strongly from observations of water–air and water–oil interfaces, where adsorption of organic solutes can cause strong decreases in interfacial tension [119–121]. The much smaller impact of organics on γ_{gw} in our system is likely related to the observation that organic adsorption at the water-CO_2 interface causes a significant displacement of adsorbed CO_2. This explanation is also consistent with findings that surface concentration has a strong influence on interfacial tension reductions [122]. Values of γ_{gw} obtained in this study generally follow the same trend as in systems without organics, except for the interface where coronene has aggregated into its own phase, where our calculated γ_{gw}-values should be interpreted with caution due to the existence of large stress fluctuations within the solid coronene aggregate (dashed black line on the right side of Figure S4C).

From the interfacial tensions at the water-CO_2 interface, γ_{gw}, and the capillary pressures in each system, we can calculate an 'effective' mineral–water-CO_2 contact angle θ_{YL} using the Young-Laplace relationship (Fig. 7B). In the absence of organics, we previously showed that θ_{YL} displays an inflection near the critical pressure of CO_2, from $\theta_{YL} \sim 0$ at low pressure to $\theta_{YL} \sim 50°$ at high pressure (gray squares in Fig. 7B); that this inflection is not reflected in the θ_{Fit}-values evaluated based on a spherical fit to the shape of the curved water-CO_2 interface (gray circles in Fig. 7B); and that the two definitions of θ can be reconciled by accounting for disjoining pressure in the adsorbed water film, [65] in agreement with other studies [123]. Despite the strong adsorption of organics at the water-CO_2 interface, the same trend in θ is observed in systems with organics, perhaps because the organic compounds examined here accumulate only at the water-CO_2 interface and minimally impact the surface tension of that interface, γ_{gw}. θ values are expected to increase at higher temperatures in quartz systems, which suggests that different organic distribution and capillary behavior may occur that are outside of the scope of this study that focuses on the larger impact of pressure on wettability variation [19,124].

3.3. Non-equilibrium properties

NEMD simulations have shown promise in revealing flow behavior, adsorption, and slip velocity at mineral-fluid interfaces [114,125]. Advancing and receding radii of curvature were gathered for each system at three different velocities of flow (Fig. 8). The fastest velocity simulations resulted in the CO_2 bubbles moving more than one full simulation cell length. During flow, the organic molecules exhibit significant redistribution. To quantify this redistribution, we define a ratio Φ that characterizes the relative abundance of organic matter at the receding and advancing ends of the CO_2 bubble.

In the quinoline and decanoic acid systems, where organics at equilibrium coat the water-CO_2 interface evenly, the receding CO_2 bubble radius of curvature generally increases with increasing bubble velocity through the pore. This correlates with an increase in the abundance of organic matter at the receding end of the CO_2 bubble (i.e., Φ greater than 1). Redistribution of the molecules coating the moving bubble to the receding end of the bubble is

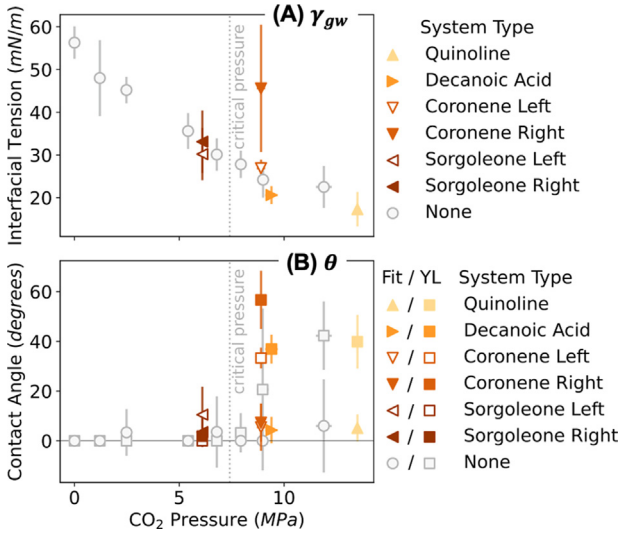

Fig. 7. Equilibrium interfacial tensions (A) and contact angles (B) as a function of CO_2 pressure. In panel B, contact angles calculated based on the curvature of the water-CO_2 interface are shown as triangles, while contact angles calculated using the Young-Laplace equation are shown as squares. The CO_2 critical pressure is marked as a dotted gray vertical line in each plot.

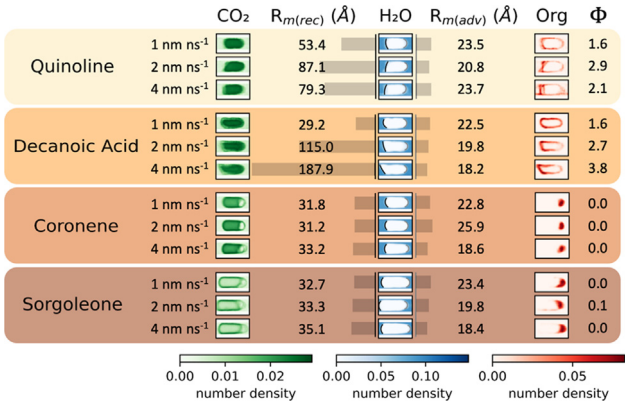

Fig. 8. Atomic density maps analogous to those in Fig. 3 obtained during NEMD simulations at three different CO_2 bubble velocities (with fluid flow from left to right). In the middle column (water density maps), the average shapes of the receding and advancing water-CO_2 interfaces are shown as black and gray lines. The corresponding radii of curvature are shown to the left and right of the water density maps column. The ratios of the abundance of organic matter on the receding and advancing ends of the CO_2 bubble (Φ) are shown in the right-most column.

expected due to the fluid flow patterns near the interface, i.e., molecules coating a flowing bubble should tend to accumulate at the rear stagnation points [126]. The bubble shape undulates most clearly in the decanoic acid system, displaying variations in adsorbed water film thickness created by flow as predicted and observed in studies with surface active agents [127–129].

In contrast, the coronene and sorgoleone systems see much smaller changes in radii of curvature at the receding end of the CO_2 bubble. The receding radii of curvature tend to increase slightly, and the advancing radii of curvature tend to decrease slightly, with increasing bubble velocity. The interfacial curvature changes at the advancing end of the bubble are similar across all four systems. Furthermore, coronene and sorgoleone remain aggregated at the *advancing* end of the bubble regardless of flow velocity. This may reflect the initial location of the coronene and sorgoleone molecules (initially aggregated on the right side of the CO_2 bubble prior to the start of the NEMD simulations). Alternatively, it may indicate a preference of distinct organic phases (formed by coronene and sorgoleone) for the most concave region of the water surface. Regardless of the origin of this effect, our results indicate that the dynamics of organic solutes and their impact on interfacial curvature during water-CO_2 multiphase flow is sensitive to the tendency of the organic molecules to form a uniform surface coating or a distinct organic phase. This novel method can also help elucidate dynamic surface tension and surface active agent concentration relationships affected by reorientation, aggregation, and clustering [130].

Based on these results, we note that the presence of organic molecules – highly likely due to the ubiquitous nature of adventitious carbon – can significantly affect dynamic wetting properties even in conditions where it does not impact the equilibrium contact angle. This suggests that measurements of dynamic wetting should take particular care to minimize or control the presence of organic molecules and that theories of dynamic wetting [131,132] should consider not only impacts associated with the redistribution of precursor water films adsorbed on solid surfaces, but also impacts associated with the redistribution of organic compounds adsorbed on the water surface. Such effects have the potential to alter the relationship between dynamic contact angles and the velocity of the three-phase contact line, [114] as evidenced by the sharp increases in receding curvatures observed with organic-coated water-CO_2 interfaces in this study. These changes in contact angle hysteresis also have potential implications for solute redistribution in circumstances involving pinning, such as in surfactant-modified colloidal droplet evaporation or the 'coffee stain' effect [133,134].

4. Conclusions

We build on our previously validated MD simulation methodologies to address a prominent source of discrepancies in contact angle observations relevant to GCS [65]. This study constitutes some of the first direct molecular-level observations of free organic solutes in $scCO_2$, water, and interfacial water films. These observations allow us to explore the affinity of various functional groups for different interfaces, and their consequential effects on wetting and flow, confirming our initial hypothesis that atomistic simulations of organic solutes can be used to evaluate capillary changes.

We find that every organic molecule studied here quickly rearranges from the mineral surface to adsorb at the water-$scCO_2$ surface. This indicates the strong preference for multi-phase flow systems with CO_2 and water to concentrate organic molecules at fluid–fluid interfaces, and to mobilize small organics. However, their behavior at the interface differs – while smaller organics tend to evenly coat the interface in a manner similar to surfactants, larger organics display a tendency to self-aggregate at the curved interface. Amongst organics coating the interface, those that are more soluble in aqueous environments can form multiple modes of hydrogen bonding with both water and the quartz surface, thus disrupting the highly structured adsorbed water film. While the organics evenly coating the water–gas interface may be expected to lower interfacial tensions in water–air systems, [119–121] the water-$scCO_2$ interfacial tensions in our study are unaffected as the organic molecules displace a volumetric equivalent of adsorbed CO_2 molecules from the surface. Upon employing non-equilibrium simulations to induce fluid flow, we find that organics coating the water-$scCO_2$ interface have a discernible impact on the receding interface shape, and accordingly on the capillary properties. These behaviors reflect observations from studies of surfactants, [116,122] organic attachment and detachment studies, [38,41,46,61,115,118] and experimental and numerical studies of surfactant-coated flowing bubbles [126–129].

The results presented have implications for the transport and redistribution of organic matter and organic contaminants in the subsurface caused by multi-phase flow and also highlight paths for future study. Future MD studies have great potential to contribute further by analyzing the molecular mechanisms at play during hydrodynamic capillary phenomena. Ideally, these future simulations will explore a wider range of organic compound chemistries and abundance, and mineral surface functional groups and surface roughness and, also, more systematically examine the influence of temperature, CO_2 density, and water-CO_2 interfacial area. These models can complement future analogous experimental studies necessary for validating these simulation results.

CRediT authorship contribution statement

Emily Wei-Hsin Sun: Conceptualization, Data curation, Formal analysis, Investigation, Methodology, Validation, Visualization, Writing - original draft, Writing - review & editing. **Ian C. Bourg:** Conceptualization, Data curation, Funding acquisition, Methodology, Resources, Writing - review & editing.

Data availability

Data will be made available on request.

Declaration of Competing Interest

The authors declare that they have no known competing financial interests or personal relationships that could have appeared to influence the work reported in this paper.

Acknowledgments

This research was supported primarily by the U.S. Department of Energy, Office of Science, Office of Basic Energy Sciences, Geosciences Program under Award DE-SC0018419. We acknowledge the support of the Natural Sciences and Engineering Research Council of Canada (NSERC), cette recherche a été financée par le Conseil de Recherches en Sciences Naturelles et en Génie du Canada (CRSNG), PGSD2-532635-2019. EWHS was additionally supported by the Mary and Randall Hack '69 Graduate Award for Water and the Environment administered by the High Meadows Environmental Institute (HMEI). MD simulations were performed using resources of the National Energy Research Scientific Computing Center (NERSC), which is supported by the U.S. Department of Energy, Office of Science, under award DE-AC02-05CH11231. The research presented here was improved by discussions with Howard Stone and Michael Celia at Princeton. The figures pre-

sented here were improved by discussions with Carolina Roe-Raymond at Princeton Research Computing. The organic molecules simulated here were constructed with the help of undergraduate HMEI summer interns Aydan Çelik and Nadia Ralston.

Appendix A. Supplementary material

Supplementary data to this article can be found online at https://doi.org/10.1016/j.jcis.2022.08.124.

Reference

[1] IPCC, 2021. *Climate Change 2021*; Masson-Delmotte, V., Zhai, P., Pirani, A., Connors, S. L., Péan, C., Berger, S., Caud, N., Chen, Y., Goldfarb, L., Gomis, M. I., Huang, M., Leitzell, K., Lonnoy, E., Matthews, J. B. R., Maycock, T. K., Waterfield, T., Yelekçi, O., Yu, R., Zhou, B., Eds.; Cambridge University Press, 2021.

[2] IPCC, 2013. *Climate Change 2013: The Physical Science Basis. Contribution of Working Group I to the Fifth Assessment Report of the Intergovernmental Panel on Climate Change*; Stocker, T. F., Qin, D., Plattner, G.-K., Tignor, M., Allen, S. K., Boschung, J., Nauels, A., Xia, Y., Bex, V., Midgley, P. M., Eds.; Cambridge University Press: Cambridge, United Kingdom and New York, NY, USA, 2013.

[3] IPCC, 2005. *IPCC Special Report on Carbon Dioxide Capture and Storage*; Metz, B.; Davidson, O.; de Coninck, H.; Loos, M.; Meyer, L., Eds.; Cambridge University Press: Cambridge, United Kingdom and New York, NY, USA, 2005.

[4] S. Fuss, W.F. Lamb, M.W. Callaghan, J. Hilaire, F. Creutzig, T. Amann, T. Beringer, W. de Oliveira Garcia, J. Hartmann, T. Khanna, G. Luderer, G.F. Nemet, J. Rogelj, P. Smith, J.L.V. Vicente, J. Wilcox, M. del Mar Zamora Dominguez, J.C. Minx, Negative Emissions—Part 2: Costs, Potentials and Side Effects, Environ. Res. Lett. 13 (6) (2018) 063002.

[5] S.M. Benson, D.R. Cole, CO2 Sequestration in Deep Sedimentary Formations, Elements 4 (5) (2008) 325–331, https://doi.org/10.2113/gselements.4.5.325.

[6] R. Juanes, C.W. MacMinn, M.L. Szulczewski, The Footprint of the CO2 Plume during Carbon Dioxide Storage in Saline Aquifers: Storage Efficiency for Capillary Trapping at the Basin Scale, Transp. Porous Media 82 (1) (2010) 19–30, https://doi.org/10.1007/s11242-009-9420-3.

[7] B. Li, S.M. Benson, Influence of Small-Scale Heterogeneity on Upward CO2 Plume Migration in Storage Aquifers, Adv. Water Resour. 83 (2015) 389–404, https://doi.org/10.1016/j.advwatres.2015.07.010.

[8] B. Zhao, C.W. MacMinn, R. Juanes, Wettability Control on Multiphase Flow in Patterned Microfluidics, Proc. Natl. Acad. Sci. 113 (37) (2016) 10251–10256, https://doi.org/10.1073/pnas.1603387113.

[9] M. Arif, S.A. Abu-Khamsin, S. Iglauer, Wettability of Rock/CO2/Brine and Rock/Oil/CO2-Enriched-Brine Systems: Critical Parametric Analysis and Future Outlook, Adv. Colloid Interface Sci. 268 (2019) 91–113, https://doi.org/10.1016/j.cis.2019.03.009.

[10] S. Iglauer, C.H. Pentland, A. Busch, CO2 Wettability of Seal and Reservoir Rocks and the Implications for Carbon Geo-Sequestration, Water Resour. Res. 51 (1) (2015) 729–774, https://doi.org/10.1002/2014WR015553.

[11] E. Skurtveit, E. Aker, M. Soldal, M. Angeli, Z. Wang, Experimental Investigation of CO2 Breakthrough and Flow Mechanisms in Shale, Pet. Geosci. 18 (1) (2012) 3–15, https://doi.org/10.1144/1354-079311-016.

[12] A. Hildenbrand, S. Schlömer, B.M. Krooss, R. Littke, Gas Breakthrough Experiments on Pelitic Rocks: Comparative Study with N2, CO2 and CH4, Geofluids 4 (1) (2004) 61–80, https://doi.org/10.1111/j.1468-8123.2004.00073.x.

[13] E. Saadatpoor, S.L. Bryant, K. Sepehrnoori, New Trapping Mechanism in Carbon Sequestration, Transp. Porous Media 82 (1) (2010) 3–17, https://doi.org/10.1007/s11242-009-9446-6.

[14] R. Pini, S.C.M. Krevor, S.M. Benson, Capillary Pressure and Heterogeneity for the CO2/Water System in Sandstone Rocks at Reservoir Conditions, Adv. Water Resour. 38 (2012) 48–59, https://doi.org/10.1016/j.advwatres.2011.12.007.

[15] D.N. Espinoza, J.C. Santamarina, Water-CO2-Mineral Systems: Interfacial Tension, Contact Angle, and Diffusion—Implications to CO2 Geological Storage, Water Resour. Res. 46 (7) (2010) 1–10, https://doi.org/10.1029/2009WR008634.

[16] E.J. Spiteri, R. Juanes, M.J. Blunt, F.M. Orr, A New Model of Trapping and Relative Permeability Hysteresis for All Wettability Characteristics, SPE J. 13 (3) (2008) 277–288, https://doi.org/10.2118/96448-PA.

[17] I.C. Bourg, L.E. Beckingham, D.J. DePaolo, The Nanoscale Basis of CO2 Trapping for Geologic Storage, Environ. Sci. Technol. 49 (17) (2015) 10265–10284, https://doi.org/10.1021/acs.est.5b03003.

[18] B. Smit, J.A. Reimer, C.M. Oldenburg, I.C. Bourg, Introduction to Carbon Capture and Sequestration, World Scientific 1 (2014), https://doi.org/10.1142/p911.

[19] M. Ali, N.K. Jha, N. Pal, A. Keshavarz, H. Hoteit, M. Sarmadivaleh, Recent Advances in Carbon Dioxide Geological Storage, Experimental Procedures, Influencing Parameters, and Future Outlook, Earth-Science Rev. 2022 (225) (October 2021), https://doi.org/10.1016/j.earscirev.2021.103895 103895.

[20] S. Iglauer, A. Salamah, M. Sarmadivaleh, K. Liu, C. Phan, Contamination of Silica Surfaces: Impact on Water-CO2-Quartz and Glass Contact Angle Measurements, Int. J. Greenh. Gas Control 22 (2014) 325–328, https://doi.org/10.1016/j.ijggc.2014.01.006.

[21] S. Iglauer, CO2–Water–Rock Wettability: Variability, Influencing Factors, and Implications for CO2 Geostorage, Acc. Chem. Res. 50 (5) (2017) 1134–1142, https://doi.org/10.1021/acs.accounts.6b00602.

[22] F. Haeri, D. Tapriyal, S. Sanguinito, F. Shi, S.J. Fuchs, L.E. Dalton, J. Baltrus, B. Howard, D. Crandall, C. Matranga, A. Goodman, CO2–Brine Contact Angle Measurements on Navajo, Nugget, Bentheimer, Bandera Brown, Berea, and Mt. Simon Sandstones, Energy Fuels 34 (5) (2020) 6085–6100, https://doi.org/10.1021/acs.energyfuels.0c00436.

[23] A.S. Al-Menhali, H.P. Menke, M.J. Blunt, S.C. Krevor, Pore Scale Observations of Trapped CO2 in Mixed-Wet Carbonate Rock: Applications to Storage in Oil Fields, Environ. Sci. Technol. 50 (18) (2016) 10282–10290, https://doi.org/10.1021/acs.est.6b03111.

[24] E.A. Al-Khdheeawi, S. Vialle, A. Barifcani, M. Sarmadivaleh, S. Iglauer, Impact of Reservoir Wettability and Heterogeneity on CO2-Plume Migration and Trapping Capacity, Int. J. Greenh. Gas Control 58 (2017) 142–158, https://doi.org/10.1016/j.ijggc.2017.01.012.

[25] J. Wan, Y. Kim, T.K. Tokunaga, Contact Angle Measurement Ambiguity in Supercritical CO2-Water-Mineral Systems: Mica as an Example, Int. J. Greenh. Gas Control 31 (2014) 128–137, https://doi.org/10.1016/j.ijggc.2014.09.029.

[26] Y.K. Kharaka, J.J. Thordsen, S.D. Hovorka, H. Seay Nance, D.R. Cole, T.J. Phelps, K.G. Knauss, Potential Environmental Issues of CO2 Storage in Deep Saline Aquifers: Geochemical Results from the Frio-I Brine Pilot Test, Texas, USA, Appl. Geochem. 24 (6) (2009) 1106–1112, https://doi.org/10.1016/j.apgeochem.2009.02.010.

[27] D.M. Akob, I.M. Cozzarelli, D.S. Dunlap, E.L. Rowan, M.M. Lorah, Organic and Inorganic Composition and Microbiology of Produced Waters from Pennsylvania Shale Gas Wells, Appl. Geochem. 60 (2015) 116–125, https://doi.org/10.1016/j.apgeochem.2015.04.011.

[28] T. Rahman, M. Lebedev, A. Barifcani, S. Iglauer, Residual Trapping of Supercritical CO2 in Oil-Wet Sandstone, J. Colloid Interface Sci. 469 (2016) 63–68, https://doi.org/10.1016/j.jcis.2016.02.020.

[29] S.R. Mihajlović, D.R. Vučinić, Z.T. Sekulić, S.Z. Milićević, B.M. Kolonja, Mechanism of Stearic Acid Adsorption to Calcite, Powder Technol. 245 (2013) 208–216, https://doi.org/10.1016/j.powtec.2013.04.041.

[30] X. Shi, R. Rosa, A. Lazzeri, On the Coating of Precipitated Calcium Carbonate with Stearic Acid in Aqueous Medium, Langmuir 26 (11) (2010) 8474–8482, https://doi.org/10.1021/la904914h.

[31] Z. Cao, M. Daly, L. Clémence, L.M. Geever, I. Major, C.L. Higginbotham, D.M. Devine, Chemical Surface Modification of Calcium Carbonate Particles with Stearic Acid Using Different Treating Methods, Appl. Surf. Sci. 378 (2016) 320–329, https://doi.org/10.1016/j.apsusc.2016.03.205.

[32] S.S. Hakim, M.H.M. Olsson, H.O. Sørensen, N. Bovet, J. Bohr, R. Feidenhans'l, S. L.S. Stipp, Interactions of the Calcite {10.4} Surface with Organic Compounds: Structure and Behaviour at Mineral–Organic Interfaces, Sci. Rep. 7 (1) (2017) 7592, https://doi.org/10.1038/s41598-017-06977-4.

[33] I.C. Bourg, Sealing Shales versus Brittle Shales: A Sharp Threshold in the Material Properties and Energy Technology Uses of Fine-Grained Sedimentary Rocks, Environ. Sci. Technol. Lett. 2 (10) (2015) 255–259, https://doi.org/10.1021/acs.estlett.5b00233.

[34] S. Iglauer, A.Z. Al-Yaseri, R. Rezaee, M. Lebedev, CO2 Wettability of Caprocks: Implications for Structural Storage Capacity and Containment Security, Geophys. Res. Lett. 42 (21) (2015) 9279–9284, https://doi.org/10.1002/2015GL065787.

[35] E.M. Thurman, Organic Geochemistry of Natural Waters; Springer Science & Business Media 2 (2012).

[36] M. Ali, F.U.R. Awan, M. Ali, A. Al-Yaseri, M. Arif, M. Sánchez-Román, A. Keshavarz, S. Iglauer, Effect of Humic Acid on CO2-Wettability in Sandstone Formation, J. Colloid Interface Sci. 588 (2021) 315–325, https://doi.org/10.1016/j.jcis.2020.12.058.

[37] T. Park, S. Yoon, J. Jung, T.-H. Kwon, Effect of Fluid-Rock Interactions on In Situ Bacterial Alteration of Interfacial Properties and Wettability of CO2–Brine–Mineral Systems for Geologic Carbon Storage, Environ. Sci. Technol. 54 (23) (2020) 15355–15365, https://doi.org/10.1021/acs.est.0c05772.

[38] M. Ali, N. Yekeen, N. Pal, A. Keshavarz, S. Iglauer, H. Hoteit, Influence of Organic Molecules on Wetting Characteristics of Mica/H2/Brine Systems: Implications for Hydrogen Structural Trapping Capacities, J. Colloid Interface Sci. 608 (2022) 1739–1749, https://doi.org/10.1016/j.jcis.2021.10.080.

[39] M.M. Thomas, J.A. Clouse, J.M. Longo, Adsorption of Organic Compounds on Carbonate Minerals, Chem. Geol. 109 (1–4) (1993) 201–213, https://doi.org/10.1016/0009-2541(93)90070-Y.

[40] M. Ali, S. Al-Anssari, M. Arif, A. Barifcani, M. Sarmadivaleh, L. Stalker, M. Lebedev, S. Iglauer, Organic Acid Concentration Thresholds for Ageing of Carbonate Minerals: Implications for CO2 Trapping/Storage, J. Colloid Interface Sci. 534 (2019) 88–94, https://doi.org/10.1016/j.jcis.2018.08.106.

[41] A. Ivanova, A. Orekhov, S. Markovic, S. Iglauer, P. Grishin, A. Cheremisin, Live Imaging of Micro and Macro Wettability Variations of Carbonate Oil Reservoirs for Enhanced Oil Recovery and CO2 Trapping/Storage, Sci. Rep. 12 (1) (2022) 1262, https://doi.org/10.1038/s41598-021-04661-2.

[42] S. Wang, Z. Tao, S.M. Persily, A.F. Clarens, CO2 Adhesion on Hydrated Mineral Surfaces, Environ. Sci. Technol. 47 (20) (2013) 11858–11865, https://doi.org/10.1021/es402199e.

[43] J. Wan, Y. Kim, T.K. Tokunaga, Contact Angle Measurement Ambiguity in Supercritical CO2–Water–Mineral Systems: Mica as an Example, Int. J.

Greenh. Gas Control 31 (2014) 128–137, https://doi.org/10.1016/j.ijggc.2014.09.029.
[44] A.M. Alhammadi, A. AlRatrout, K. Singh, B. Bijeljic, M.J. Blunt, In Situ Characterization of Mixed-Wettability in a Reservoir Rock at Subsurface Conditions, Sci. Rep. 7 (1) (2017) 10753, https://doi.org/10.1038/s41598-017-10992-w.
[45] S.R. Holmes-Farley, C.D. Bain, G.M. Whitesides, Wetting of Functionalized Polyethylene Film Having Ionizable Organic Acids and Bases at the Polymer-Water Interface: Relations between Functional Group Polarity, Extent of Ionization, and Contact Angle with Water, Langmuir 4 (4) (1988) 921–937, https://doi.org/10.1021/la00082a025.
[46] A. Ivanova, N. Mitiurev, A. Cheremisin, A. Orekhov, R. Kamyshinsky, A. Vasiliev, Characterization of Organic Layer in Oil Carbonate Reservoir Rocks and Its Effect on Microscale Wetting Properties, Sci. Rep. 9 (1) (2019) 10667, https://doi.org/10.1038/s41598-019-47139-y.
[47] S. Leroch, M. Wendland, Simulation of Forces between Humid Amorphous Silica Surfaces: A Comparison of Empirical Atomistic Force Fields, J. Phys. Chem. C 116 (50) (2012) 26247–26261, https://doi.org/10.1021/jp302428b.
[48] E.J.W. Wensink, A.C. Hoffmann, M.E.F. Apol, H.J.C. Berendsen, Properties of Adsorbed Water Layers and the Effect of Adsorbed Layers on Interparticle Forces by Liquid Bridging, Langmuir 16 (19) (2000) 7392–7400, https://doi.org/10.1021/la000009e.
[49] B. Rotenberg, A.J. Patel, D. Chandler, Molecular Explanation for Why Talc Surfaces Can Be Both Hydrophilic and Hydrophobic, J. Am. Chem. Soc. 133 (50) (2011) 20521–20527, https://doi.org/10.1021/ja208687a.
[50] M. Khalkhali, N. Kazemi, H. Zhang, Q. Liu, Wetting at the Nanoscale: A Molecular Dynamics Study, J. Chem. Phys. 146 (11) (2017), https://doi.org/10.1063/1.4978497 114704.
[51] Q. Liu, J. Yu, H. Wang, The Role of the Substrate Roughness in Contact Angle Hysteresis and Dynamic Deviation, Int. J. Heat Mass Transf. 148 (2020), https://doi.org/10.1016/j.ijheatmasstransfer.2019.118985 118985.
[52] R.T. Cygan, J.A. Greathouse, A.G. Kalinichev, Advances in Clayff Molecular Simulation of Layered and Nanoporous Materials and Their Aqueous Interfaces, J. Phys. Chem. C 125 (32) (2021) 17573–17589, https://doi.org/10.1021/acs.jpcc.1c04600.
[53] D. Argyris, D.R. Cole, A. Striolo, Hydration Structure on Crystalline Silica Substrates, Langmuir 25 (14) (2009) 8025–8035, https://doi.org/10.1021/la9005136.
[54] A. Abramov, A. Keshavarz, S. Iglauer, Wettability of Fully Hydroxylated and Alkylated (001) α-Quartz Surface in Carbon Dioxide Atmosphere, J. Phys. Chem. C 123 (14) (2019) 9027–9040, https://doi.org/10.1021/acs.jpcc.9b00263.
[55] A. Abramov, S. Iglauer, Application of the CLAYFF and the DREIDING Force Fields for Modeling of Alkylated Quartz Surfaces, Langmuir 35 (17) (2019) 5746–5752, https://doi.org/10.1021/acs.langmuir.9b00527.
[56] X. Li, Q. Xue, T. Wu, Y. Jin, C. Ling, S. Lu, Oil Detachment from Silica Surface Modified by Carboxy Groups in Aqueous Cetyltriethylammonium Bromide Solution, Appl. Surf. Sci. 353 (2015) 1103–1111, https://doi.org/10.1016/j.apsusc.2015.07.014.
[57] Q. Liu, S. Yuan, H. Yan, X. Zhao, Mechanism of Oil Detachment from a Silica Surface in Aqueous Surfactant Solutions: Molecular Dynamics Simulations, J. Phys. Chem. B 116 (9) (2012) 2867–2875, https://doi.org/10.1021/jp2118482.
[58] H. Yan, S. Yuan, Molecular Dynamics Simulation of the Oil Detachment Process within Silica Nanopores, J. Phys. Chem. C 120 (5) (2016) 2667–2674, https://doi.org/10.1021/acs.jpcc.5b09841.
[59] E. Lowry, M. Sedghi, L. Goual, Molecular Simulations of NAPL Removal from Mineral Surfaces Using Microemulsions and Surfactants, Colloids Surf. A Physicochem. Eng. Asp. 506 (2016) 485–494, https://doi.org/10.1016/j.colsurfa.2016.07.002.
[60] S. Bai, J. Kubelka, M. Piri, Atomistic Molecular Dynamics Simulations of Surfactant-Induced Wettability Alteration in Crevices of Calcite Nanopores, Energy & Fuels 34 (3) (2020) 3135–3143, https://doi.org/10.1021/acs.energyfuels.9b04528.
[61] T. Fang, M. Wang, C. Wang, B. Liu, Y. Shen, C. Dai, J. Zhang, Oil Detachment Mechanism in CO2 Flooding from Silica Surface: Molecular Dynamics Simulation, Chem. Eng. Sci. 164 (2017) 17–22, https://doi.org/10.1016/j.ces.2017.01.067.
[62] S. Wang, F. Javadpour, Q. Feng, Molecular Dynamics Simulations of Oil Transport through Inorganic Nanopores in Shale, Fuel 171 (2016) 74–86, https://doi.org/10.1016/j.fuel.2015.12.071.
[63] M.M. Koleini, M.H. Badizad, H. Mahani, A.M. Dastjerdi, S. Ayatollahi, M.H. Ghazanfari, Atomistic Insight into Salinity Dependent Preferential Binding of Polar Aromatics to Calcite/Brine Interface: Implications to Low Salinity Waterflooding, Sci. Rep. 11 (1) (2021) 11967, https://doi.org/10.1038/s41598-021-91402-0.
[64] T. Underwood, V. Erastova, P. Cubillas, H.C. Greenwell, Molecular Dynamic Simulations of Montmorillonite Organic Interactions under Varying Salinity: An Insight into Enhanced Oil Recovery, J. Phys. Chem. C 119 (13) (2015) 7282–7294, https://doi.org/10.1021/acs.jpcc.5b00555.
[65] E.W.-H. Sun, I.C. Bourg, Molecular Dynamics Simulations of Mineral Surface Wettability by Water Versus CO2: Thin Films, Contact Angles, and Capillary Pressure in a Silica Nanopore, J. Phys. Chem. C 124 (46) (2020) 25382–25395, https://doi.org/10.1021/acs.jpcc.0c07948.
[66] M. Tuller, D. Or, L.M. Dudley, Adsorption and Capillary Condensation in Porous Media: Liquid Retention and Interfacial Configurations in Angular Pores, Water Resour. Res. 35 (7) (1999) 1949–1964, https://doi.org/10.1029/1999WR900098.
[67] M. Tang, D.J. Cziczo, V.H. Grassian, Interactions of Water with Mineral Dust Aerosol: Water Adsorption, Hygroscopicity, Cloud Condensation, and Ice Nucleation, Chem. Rev. 116 (7) (2016) 4205–4259, https://doi.org/10.1021/acs.chemrev.5b00529.
[68] Z. Wang, M. Elimelech, S. Lin, Environmental Applications of Interfacial Materials with Special Wettability, Environ. Sci. Technol. 50 (5) (2016) 2132–2150, https://doi.org/10.1021/acs.est.5b04351.
[69] X. Yao, Y. Song, L. Jiang, Applications of Bio-Inspired Special Wettable Surfaces, Adv. Mater. 23 (6) (2011) 719–734, https://doi.org/10.1002/adma.201002689.
[70] C. Boo, S. Hong, M. Elimelech, Relating Organic Fouling in Membrane Distillation to Intermolecular Adhesion Forces and Interfacial Surface Energies, Environ. Sci. Technol. 52 (24) (2018) 14198–14207, https://doi.org/10.1021/acs.est.8b05768.
[71] F. Mugele, J.-C. Baret, Electrowetting: From Basics to Applications, J. Phys. Condens. Matter 17 (28) (2005) R705–R774, https://doi.org/10.1088/0953-8984/17/28/R01.
[72] J.B.T. Scott, R.D. Barker, Characterization of Sandstone by Electrical Spectroscopy for Stratigraphical and Hydrogeological Investigations, Q. J. Eng. Geol. Hydrogeol. 38 (2) (2005) 143–154, https://doi.org/10.1144/1470-9326/04-036.
[73] F. Al Saadi, K.-H. Wolf, C. van Kruijsdijk, Characterization of Fontainebleau Sandstone: Quartz Overgrowth and Its Impact on Pore-Throat Framework, J. Pet. Environ. Biotechnol. 08 (03) (2017), https://doi.org/10.4172/2157-7463.1000328.
[74] I. Gaus, M. Azaroual, I. Czernichowski-Lauriol, Reactive Transport Modelling of the Impact of CO2 Injection on the Clayey Cap Rock at Sleipner (North Sea), Chem. Geol. 217 (3–4) (2005) 319–337, https://doi.org/10.1016/j.chemgeo.2004.12.016.
[75] M. Wigand, J.W. Carey, H. Schütt, E. Spangenberg, J. Erzinger, Geochemical Effects of CO2 Sequestration in Sandstones under Simulated in Situ Conditions of Deep Saline Aquifers, Appl. Geochem. 23 (9) (2008) 2735–2745, https://doi.org/10.1016/j.apgeochem.2008.06.006.
[76] V.N. Balashov, G.D. Guthrie, J.A. Hakala, C.L. Lopano, J.D. Rimstidt, S.L. Brantley, Predictive Modeling of CO2 Sequestration in Deep Saline Sandstone Reservoirs: Impacts of Geochemical Kinetics, Appl. Geochem. 30 (2013) 41–56, https://doi.org/10.1016/j.apgeochem.2012.08.016.
[77] F. Alnili, A. Al-Yaseri, H. Roshan, T. Rahman, M. Verall, M. Lebedev, M. Sarmadivaleh, S. Iglauer, A. Barifcani, Carbon Dioxide/Brine Wettability of Porous Sandstone versus Solid Quartz: An Experimental and Theoretical Investigation, J. Colloid Interface Sci. 524 (2018) 188–194, https://doi.org/10.1016/j.jcis.2018.04.029.
[78] K. Kihara, An X-Ray Study of the Temperature Dependence of the Quartz Structure, Eur. J. Mineral. 2 (1) (1990) 63–78, https://doi.org/10.1127/ejm/2/1/0063.
[79] M.L. Schlegel, K.L. Nagy, P. Fenter, N.C. Sturchio, Structures of Quartz (100)- and (101)-Water Interfaces Determined by X-Ray Reflectivity and Atomic Force Microscopy of Natural Growth Surfaces, Geochim. Cosmochim. Acta 66 (17) (2002) 3037–3054, https://doi.org/10.1016/S0016-7037(02)00912-2.
[80] A. Silvestri, E. Ataman, A. Budi, S.L.S. Stipp, J.D. Gale, P. Raiteri, Wetting Properties of the CO2–Water–Calcite System via Molecular Simulations: Shape and Size Effects, Langmuir 35 (50) (2019) 16669–16678, https://doi.org/10.1021/acs.langmuir.9b02881.
[81] A. Amirfazli, A.W. Neumann, Status of the Three-Phase Line Tension: A Review, Adv. Colloid Interface Sci. 110 (3) (2004) 121–141, https://doi.org/10.1016/j.cis.2004.05.001.
[82] R. Bey, B. Coasne, C. Picard, Carbon Dioxide as a Line Active Agent: Its Impact on Line Tension and Nucleation Rate, Proc. Natl. Acad. Sci. 118 (33) (2021), https://doi.org/10.1073/pnas.2102449118 e2102449118.
[83] M.J. Baedecker, I.M. Cozzarelli, R.P. Eganhouse, D.I. Siegel, P.C. Bennett, Crude Oil in a Shallow Sand and Gravel Aquifer—III. Biogeochemical Reactions and Mass Balance Modeling in Anoxic Groundwater, Appl. Geochem. 8 (6) (1993) 569–586, https://doi.org/10.1016/0883-2927(93)90014-8.
[84] J.M. Zachara, C.C. Ainsworth, L.J. Felice, C.T. Resch, Quinoline Sorption to Subsurface Materials: Role of pH and Retention of the Organic Cation, Environ. Sci. Technol. 20 (6) (1986) 620–627, https://doi.org/10.1021/es00148a013.
[85] J.A. Leenheer, T.I. Noyes, H.A. Stuber, Determination of Polar Organic Solutes in Oil-Shale Retort Water, Environ. Sci. Technol. 16 (10) (1982) 714–723, https://doi.org/10.1021/es00104a015.
[86] S.H. Standal, A.M. Blokhus, J. Haavik, A. Skauge, T. Barth, Partition Coefficients and Interfacial Activity for Polar Components in Oil/Water Model Systems, J. Colloid Interface Sci. 212 (1) (1999) 33–41, https://doi.org/10.1006/jcis.1998.5988.
[87] L.F. Zubeir, D.J.G.P. van Osch, M.A.A. Rocha, F. Banat, M.C. Kroon, Carbon Dioxide Solubilities in Decanoic Acid-Based Hydrophobic Deep Eutectic Solvents, J. Chem. Eng. Data 63 (4) (2018) 913–919, https://doi.org/10.1021/acs.jced.7b00534.
[88] M. Keiluweit, M. Kleber, Molecular-Level Interactions in Soils and Sediments: The Role of Aromatic π-Systems, Environ. Sci. Technol. 43 (10) (2009) 3421–3429, https://doi.org/10.1021/es8033044.
[89] T. Bakshi, V. Vishal, A Review on the Role of Organic Matter in Gas Adsorption in Shale, Energy and Fuels 35 (19) (2021) 15249–15264, https://doi.org/10.1021/acs.energyfuels.1c01631.

[90] S. Mohd Amin, D.J. Weiss, M.J. Blunt, Reactive Transport Modelling of Geologic CO2 Sequestration in Saline Aquifers: The Influence of Pure CO2 and of Mixtures of CO2 with CH4 on the Sealing Capacity of Cap Rock at 37 °C and 100 bar, Chem. Geol. 367 (2014) 39–50, https://doi.org/10.1016/j.chemgeo.2014.01.002.
[91] National Center for Biotechnology Information. PubChem Compound Summary for CID 7047, Quinoline https://pubchem.ncbi.nlm.nih.gov/compound/Quinoline (accessed Feb 10, 2022).
[92] National Center for Biotechnology Information. PubChem Compound Summary for CID 2969, Decanoic acid https://pubchem.ncbi.nlm.nih.gov/compound/Decanoic-acid (accessed Feb 10, 2022).
[93] D. Mackay, W.Y. Shiu, Aqueous Solubility of Polynuclear Aromatic Hydrocarbons, J. Chem. Eng. Data 22 (4) (1977) 399–402, https://doi.org/10.1021/je60075a012.
[94] M.M. Trezzi, R.A. Vidal, D.P. Dick, M.C.R. Peralba, N.D. Kruse, Sorptive Behavior of Sorgoleone in Ultisol in Two Solvent Systems and Determination of Its Lipophilicity, J. Environ. Sci. Heal. Part B Pestic. Food Contam. Agric. Wastes 41 (4) (2006) 345–356, https://doi.org/10.1080/03601230600613780.
[95] U. Blum, Plant-Plant Allelopathic Interactions III, Springer, 2019.
[96] R.T. Cygan, J.-J. Liang, A.G. Kalinichev, Molecular Models of Hydroxide, Oxyhydroxide, and Clay Phases and the Development of a General Force Field, J. Phys. Chem. B 108 (4) (2004) 1255–1266, https://doi.org/10.1021/jp0363287.
[97] H.J.C. Berendsen, J.R. Grigera, T.P. Straatsma, The Missing Term in Effective Pair Potentials, J. Phys. Chem. 91 (24) (1987) 6269–6271, https://doi.org/10.1021/j100308a038.
[98] J.G. Harris, K.H. Yung, Carbon Dioxide's Liquid-Vapor Coexistence Curve And Critical Properties as Predicted by a Simple Molecular Model, J. Phys. Chem. 99 (31) (1995) 12021–12024, https://doi.org/10.1021/j100031a034.
[99] W.L. Jorgensen, D.S. Maxwell, J. Tirado-Rives, Development and Testing of the OPLS All-Atom Force Field on Conformational Energetics and Properties of Organic Liquids, J. Am. Chem. Soc. 118 (45) (1996) 11225–11236, https://doi.org/10.1021/ja9621760.
[100] A.I. Jewett, D. Stelter, J. Lambert, S.M. Saladi, O.M. Roscioni, M. Ricci, L. Autin, M. Maritan, S.M. Bashusqeh, T. Keyes, R.T. Dame, J.-E. Shea, G.J. Jensen, D.S. Goodsell, Moltemplate: A Tool for Coarse-Grained Modeling of Complex Biological Matter and Soft Condensed Matter Physics, J. Mol. Biol. 433 (11) (2021), https://doi.org/10.1016/j.jmb.2021.166841 166841.
[101] M. In Het Panhuis, C.H. Patterson, R.M. Lynden-Bell, A Molecular Dynamics Study of Carbon Dioxide in Water: Diffusion, Structure and Thermodynamics, Mol. Phys, 94 (6) (1998), 963–972, doi:10.1080/002689798167539.
[102] G. Hura, D. Russo, R.M. Glaeser, T. Head-Gordon, M. Krack, M. Parrinello, Water Structure as a Function of Temperature from X-Ray Scattering Experiments and Ab Initio Molecular Dynamics, Phys. Chem. Chem. Phys. 5 (10) (2003) 1981, https://doi.org/10.1039/b301481a.
[103] J.R. Errington, A.Z. Panagiotopoulos, A Fixed Point Charge Model for Water Optimized to the Vapor−Liquid Coexistence Properties, J. Phys. Chem. B 102 (38) (1998) 7470–7475, https://doi.org/10.1021/jp982068v.
[104] C. Vega, J.L.F. Abascal, Simulating Water with Rigid Non-Polarizable Models: A General Perspective, Phys. Chem. Chem. Phys. 13 (44) (2011) 19663, https://doi.org/10.1039/c1cp22168j.
[105] J. Vorholz, V.I. Harismiadis, B. Rumpf, A.Z. Panagiotopoulos, G. Maurer, Vapor +liquid Equilibrium of Water, Carbon Dioxide, and the Binary System, Water +Carbon Dioxide, from Molecular Simulation, Fluid Phase Equilib. 170 (2) (2000) 203–234, https://doi.org/10.1016/S0378-3812(00)00315-0.
[106] A.A. Skelton, P. Fenter, J.D. Kubicki, D.J. Wesolowski, P.T. Cummings, Simulations of the Quartz(10$\bar{1}$1)/Water Interface: A Comparison of Classical Force Fields, Ab Initio Molecular Dynamics, and X-Ray Reflectivity Experiments, J. Phys. Chem. C 115 (5) (2011) 2076–2088, https://doi.org/10.1021/jp109446d.
[107] I.C. Bourg, C.I. Steefel, Molecular Dynamics Simulations of Water Structure and Diffusion in Silica Nanopores, J. Phys. Chem. C 116 (21) (2012) 11556–11564, https://doi.org/10.1021/jp301299a.
[108] L.C. Nielsen, I.C. Bourg, G. Sposito, Predicting CO2-Water Interfacial Tension under Pressure and Temperature Conditions of Geologic CO2 Storage, Geochim. Cosmochim. Acta 81 (2012) 28–38, https://doi.org/10.1016/j.gca.2011.12.018.
[109] H. Jiang, I.G. Economou, A.Z. Panagiotopoulos, Molecular Modeling of Thermodynamic and Transport Properties for CO2 and Aqueous Brines, Acc. Chem. Res. 50 (4) (2017) 751–758, https://doi.org/10.1021/acs.accounts.6b00632.
[110] T.R. Underwood, H.C. Greenwell, The Water-Alkane Interface at Various NaCl Salt Concentrations: A Molecular Dynamics Study of the Readily Available Force Fields, Sci. Rep. 8 (1) (2018) 352, https://doi.org/10.1038/s41598-017-18633-y.
[111] Y. Liang, S. Tsuji, J. Jia, T. Tsuji, T. Matsuoka, Modeling CO2–Water–Mineral Wettability and Mineralization for Carbon Geosequestration, Acc. Chem. Res. 50 (7) (2017) 1530–1540, https://doi.org/10.1021/acs.accounts.7b00049.
[112] J.A.R. Willemsen, S.C.B. Myneni, I.C. Bourg, Molecular Dynamics Simulations of the Adsorption of Phthalate Esters on Smectite Clay Surfaces, J. Phys. Chem. C 123 (22) (2019) 13624–13636, https://doi.org/10.1021/acs.jpcc.9b01864.
[113] S. Plimpton, Fast Parallel Algorithms for Short-Range Molecular Dynamics, J. Comput. Phys. 117 (1) (1995) 1–19, https://doi.org/10.1006/jcph.1995.1039.
[114] P. Huang, L. Shen, Y. Gan, F. Maggi, A. El-Zein, Z. Pan, Atomistic Study of Dynamic Contact Angles in CO2–Water–Silica System, Langmuir 35 (15) (2019) 5324–5332, https://doi.org/10.1021/acs.langmuir.9b00076.
[115] D.L. Lord, A.H. Demond, K.F. Hayes, Effects of Organic Base Chemistry on Interfacial Tension, Wettability, and Capillary Pressure in Multiphase Subsurface Waste Systems, Transp. Porous Media 38 (1–2) (2000) 79–92, https://doi.org/10.1023/A:1006659116417.
[116] K.J. Stebe, D. Barthès-Biesel, Marangoni Effects of Adsorption—Desorption Controlled Surfactants on the Leading End of an Infinitely Long Bubble in a Capillary, J. Fluid Mech. 286 (12) (1995) 25–48, https://doi.org/10.1017/S0022112095000632.
[117] G. Rother, S. Gautam, T. Liu, D.R. Cole, A. Busch, A.G. Stack, Molecular Structure of Adsorbed Water Phases in Silica Nanopores, J. Phys. Chem. C 126 (5) (2022) 2885–2895, https://doi.org/10.1021/acs.jpcc.1c10162.
[118] Q.R.S. Miller, J.P. Kaszuba, H.T. Schaef, M.E. Bowden, B.P. McGrail, Impacts of Organic Ligands on Forsterite Reactivity in Supercritical CO2 Fluids, Environ. Sci. Technol. 49 (7) (2015) 4724–4734, https://doi.org/10.1021/es506065d.
[119] D.L. Lord, K.F. Hayes, A.H. Demond, A. Salehzadeh, Influence of Organic Acid Solution Chemistry on Subsurface Transport Properties. 1. Surface and Interfacial Tension, Environ. Sci. Technol. 31 (7) (1997) 2045–2051, https://doi.org/10.1021/es960854c.
[120] P.C. Hiemenz, R. Rajagopalan, Principles of Colloid and Surface Chemistry, Revised and Expanded, CRC Press, Third Edit., 2016.
[121] M.J. Rosen, J.T. Kunjappu, Surfactants and Interfacial Phenomena, John Wiley & Sons, 2012.
[122] C. Jian, M.R. Poopari, Q. Liu, N. Zerpa, H. Zeng, T. Tang, Reduction of Water/Oil Interfacial Tension by Model Asphaltenes: The Governing Role of Surface Concentration, J. Phys. Chem. B 120 (25) (2016) 5646–5654, https://doi.org/10.1021/acs.jpcb.6b03691.
[123] Z. Qin, E. Barsotti, M. Piri, Sub-Nanometer Scale Investigation of in Situ Wettability Using Environmental Transmission Electron Microscopy, J. Colloid Interface Sci. 593 (2021) 266–275, https://doi.org/10.1016/j.jcis.2021.02.075.
[124] M. Arif, A. Barifcani, S. Iglauer, Solid/CO2 and Solid/Water Interfacial Tensions as a Function of Pressure, Temperature, Salinity and Mineral Type: Implications for CO2-Wettability and CO2 Geo-Storage, Int. J. Greenh. Gas Control 53 (2016) 263–273, https://doi.org/10.1016/j.ijggc.2016.08.020.
[125] T. Wu, D. Zhang, Impact of Adsorption on Gas Transport in Nanopores, Sci. Rep. 6 (1) (2016) 23629, https://doi.org/10.1038/srep23629.
[126] Y.E. Yu, S. Khodaparast, H.A. Stone, Armoring Confined Bubbles in the Flow of Colloidal Suspensions, Soft Matter 13 (15) (2017) 2857–2865, https://doi.org/10.1039/C6SM02585D.
[127] Z.Y. Luo, B.F. Bai, Retardation of Droplet Transport in Confined Microchannel by Interfacial Jamming of Nanoparticles, Phys. Fluids 32 (8) (2020), https://doi.org/10.1063/5.0016450 087110.
[128] Z.Y. Luo, X.L. Shang, B.F. Bai, Effect of Soluble Surfactant on the Motion of a Confined Droplet in a Square Microchannel, Phys. Fluids 31 (11) (2019), https://doi.org/10.1063/1.5125949 117104.
[129] C.-W. Park, Influence of Soluble Surfactants on the Motion of a Finite Bubble in a Capillary Tube, Phys. Fluids A Fluid Dyn. 4 (11) (1992) 2335–2347, https://doi.org/10.1063/1.858475.
[130] V.B. Fainerman, R. Miller, E.V. Aksenenko, Simple Model for Prediction of Surface Tension of Mixed Surfactant Solutions, Adv. Colloid Interface Sci. 96 (1–3) (2002) 339–359, https://doi.org/10.1016/S0001-8686(01)00088-4.
[131] H. A, Z. Yang, R. Hu, Y.-F. Chen, Roles of Energy Dissipation and Asymmetric Wettability in Spontaneous Imbibition Dynamics in a Nanochannel, J. Colloid Interface Sci. 607 (2022) 1023–1035, https://doi.org/10.1016/j.jcis.2021.09.051.
[132] W. Tian, K. Wu, Z. Chen, Z. Lei, Y. Gao, Z. Chen, Y. Liu, Y. Hou, Q. Zhu, J. Li, Dynamic Wetting of Solid-Liquid-Liquid System by Molecular Kinetic Theory, J. Colloid Interface Sci. 579 (2020) 470–478, https://doi.org/10.1016/j.jcis.2020.06.101.
[133] Y. Li, C. Diddens, T. Segers, H. Wijshoff, M. Versluis, D. Lohse, Evaporating Droplets on Oil-Wetted Surfaces: Suppression of the Coffee-Stain Effect, Proc. Natl. Acad. Sci. 117 (29) (2020) 16756–16763, https://doi.org/10.1073/pnas.2006153117.
[134] Y.-F. Li, Y.-J. Sheng, H.-K. Tsao, Solute Concentration-Dependent Contact Angle Hysteresis and Evaporation Stains, Langmuir 30 (26) (2014) 7716–7723, https://doi.org/10.1021/la501438k.